

1 Identification of potential molecules against COVID-19 main 2 protease through structure-guided virtual screening approach

3 Lovika Mittal^{1,#}, Anita Kumari^{1,#}, Mitul Srivastava^{1,#}, Mrityunjay Singh¹, Shailendra Asthana^{1*}

4 ¹ Translational Health Science and Technology Institute (THSTI), Haryana, 121001, India

5
6
7 # These authors contributed equally

8 * To whom the correspondence should be addressed.

9 10 **Dr. Shailendra Asthana**

11 Translational Health Science and Technology Institute (THSTI),

12 NCR Biotech Science Cluster, 3rd Milestone

13 Faridabad – Gurgaon Expressway, Haryana-121001, India

14 E-Mail: sasthana@thsti.res.in

15 16 **Abstract**

17 The epidemic caused by novel coronavirus disease 2019 (COVID-19) infecting around ~ 1
18 million populations worldwide and counting, has demanded quick and potential therapeutic
19 strategies. Current approved drugs or molecules under clinical trials can be a good pool for
20 repurposing through computer-aided drug design techniques to quickly identify promising
21 drug repurposing candidates. The structural information of recently released crystal structure
22 of COVID-19 main protease (M^{Pro}) in complex with inhibitor, N3, and 13b molecules was
23 utilized to conduct extensive virtual docking screening of aforementioned drug pool.
24 Considering the recent success of HIV protease molecules, we also used protease molecules
25 (from different viruses) for drug repurposing purposes. The top docking hits were further
26 used for focused docking followed by binding free energy calculations using MM-GBSA.
27 Interestingly, in our screening, several promising already documented drugs stand out as
28 potential inhibitors of COVID-19 (M^{Pro}). However, based on N3 and 13B molecules as
29 control, we have identified six potential molecules, Leupeptin Hemisulphate, Pepstatin A,
30 Nelfinavir, Birinapant, Lypressin and Octeotide which have shown the docking energy > -
31 8.0 kcal/mol and MMGBSA > -68.0 kcal/mol. The pharmacokinetic annotations and
32 therapeutic importance of these molecules have suggested that they possess drug-like
33 properties and pave their way for in vitro studies. Further insight shows that the molecules
34 forms stable interactions with *hot-spot* residues, that are mainly conserved and can be
35 targeted for structure and pharmacophore-based designing of more potent molecules.

36
37 **Key-words: Virtual screening, COVID-19, SARS-CoV-2, M^{Pro} protease, molecular**
38 **docking analysis, binding free energy.**

1 1. Introduction

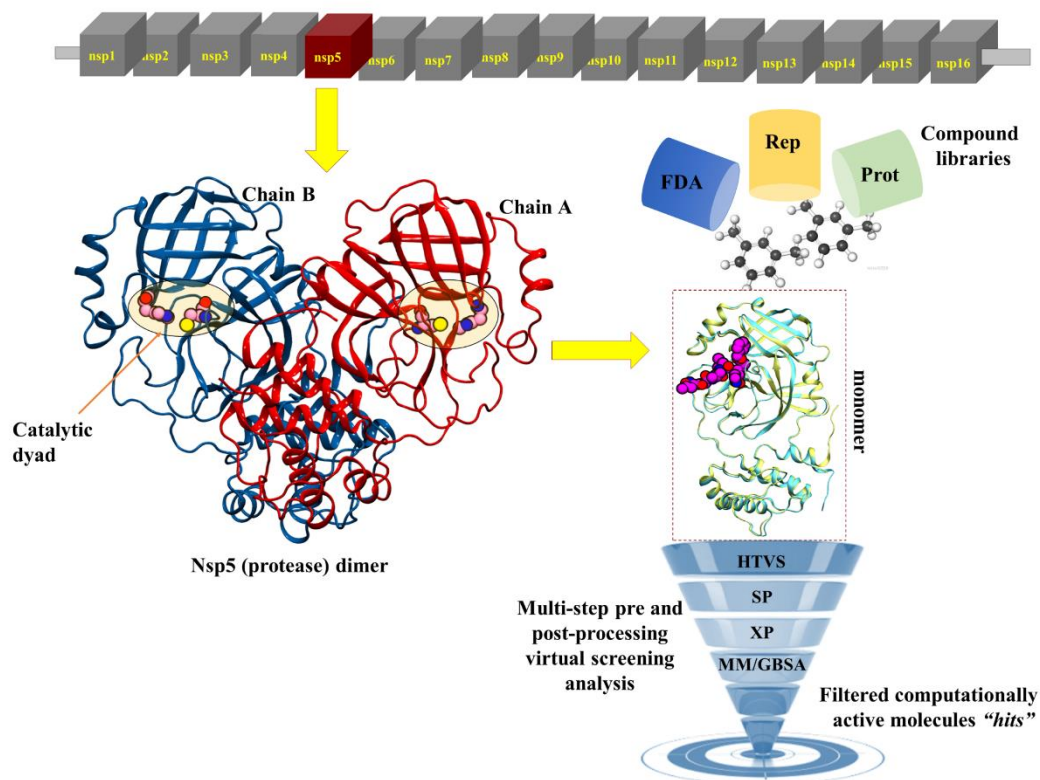
2 Coronaviruses (CoVs) belong to a pathogenic group of viruses that causes respiratory tract
3 infections in mammals and birds. It originated through zoonotic transmission between bats
4 and humans and then transmitted from humans to humans spreading via saliva droplets or
5 nasal discharge from an infected person (*Coronavirus*, n.d.). It belongs to a family of
6 coronaviridae and they can be divided into four genera, i.e., alphacoronavirus,
7 betacoronavirus, gammacoronavirus, and deltacoronavirus. The current outbreak of
8 coronavirus disease (COVID-19; previously known as 2019-nCoV-2) was first reported from
9 Wuhan, China, in late December 2019 (H. Chen et al., 2020), which has subsequently
10 affected countries worldwide, reporting nearly half a million of confirmed cases of COVID-
11 19 along with ~39,000 deaths and nearly 200,000 people have recovered as per data recorded
12 in march 2020 (*Coronavirus Update (Live): 803,772 Cases and 39,070 Deaths from COVID-
13 19 Virus Outbreak - Worldometer*, n.d.). Human coronaviruses were initially discovered in
14 the 1960s (Kahn & McIntosh, 2005) with a bronchitis infection in chickens and in humans.
15 SARS-CoV (in 2003), HCoV NL63 (2004), HKU1 (2005), MERS-CoV (2012) and SARS-
16 CoV-2 (COVID-19) are members of its family that have been identified till now (Su et al.,
17 2016). The COVID-19 is a new strain that has emerged due to which they are not familiar to
18 our immune system causing infection in the respiratory tract. According to WHO, the
19 symptoms include mild to moderate respiratory illness and in severe conditions may develop
20 difficulty in breathing and pain in chest, but patients may recover without special treatment.
21 Old age people with medical complications like cardiovascular disease, diabetes, chronic
22 respiratory disease, and cancer are known to be more likely to develop serious illness.

23 Unfortunately, at present there is no well-defined treatment or therapeutics against COVID-
24 19 is available but the preventive measures are being recommended worldwide which
25 includes social distancing and isolation of infected individuals along with providing treatment
26 as per the symptoms with mild disease and oxygen therapy/ventilator support for patients
27 with severe disease. However, the clinical trials for already marketed drugs such as lopinavir,
28 ritonavir, hydroxychloroquine, azithromycin, (Tirumalaraju, 2020c) chloroquine
29 (*Chloroquine/ Hydroxychloroquine Prevention of Coronavirus Disease (COVID-19) in the
30 Healthcare Setting - Full Text View - ClinicalTrials.gov*, n.d.), Remdesivir (Tirumalaraju,
31 2020b) etc. along with antibiotics are being evaluated to treat the secondary infections
32 (www.clinicaltrials.gov). All of the drug options come from experience treating SARS,
33 MERS or some other new influenza virus previously (Lu, 2020). These drugs would be
34 helpful but the efficacy needs to be further confirmed. Few COVID-19 vaccines are also
35 under clinical trials such as Moderna's mRNA-1273, first US clinical vaccine funded by
36 NIH's NIAID (National Institute of Allergy and Infectious Diseases) (Tirumalaraju,
37 2020a). Thus, there is an unmet requirement for the specific anti-COVID-19 therapeutics to
38 limit the severity of the deadly disease. Various clinicians and researchers are engaged in
39 investigating and developing antivirals using different strategies combining experimental and
40 *in-silico* approaches (Ahmed et al., n.d.; Hatada et al., n.d.; Nair & Narayanan, n.d.) with the
41 goal of identifying novel, selective and potent therapeutic agents. The RCSB protein data
42 bank (PDB) (www.rcsb.org) has collected ~104 crystal structures of COVID-19 proteins to
43 allow the rational designing of small molecules. COVID-19 (or SARS-CoV-2) is an
44 enveloped non-segmented large (+)ssRNA virus (~30kb) with 5'-cap structure and 3'-poly-A
45 tail belonging to β -CoV category (Casella et al., 2020; Su et al., 2016). It is round or elliptic
46 or pleomorphic with diameter ranging in 60–140 nm (Casella et al., 2020). It is presumed
47 that like other CoVs, it is sensitive to ultraviolet rays and heat. Moreover, these viruses could
48 be effectively inactivated by lipid solvents including ether (75%), ethanol, chlorine-

1 containing disinfectant, peroxyacetic acid and chloroform except for chlorhexidine(Cascella
2 et al., 2020) Its RNA genome contains 29891 nucleotides, and encoding for ~9860 amino
3 acids (Cascella et al., 2020). The genome codes for both structural (namely, spike (S),
4 envelope (E), membrane (M) and nucleocapsid (N)) and non-structural proteins (NSPs 1-16)
5 (Graham et al., 2008).

6 Its replicase gene encodes two overlapping polyproteins pp1a and pp1ab, that are required for
7 viral replication and transcription. Its first ORF (orf1) is the largest, that encodes ~ 70% of
8 its entire genome and 16 NSPs (Bzówka et al., n.d.; Y. Chen et al., 2020). Among these nsp5,
9 the main protease (Mpro, also known as a chymotrypsin-like cysteine protease 3CLpro),
10 encoded by nsp5, has been found to play a fundamental role in viral gene expression and
11 replication, thus it became an attractive target for anti-CoV drug design (Bzówka et al., n.d.;
12 Y. Chen et al., 2020). The remaining ORFs are responsible to code for accessory and
13 structural proteins. The functional polypeptides are released from the polyproteins by
14 extensive proteolytic processing via 33.8-kDa main protease (M^{pro}). M^{pro} digests the
15 polyprotein at 11 conserved sites, starting with the autolytic cleavage of this enzyme itself
16 from pp1a and pp1ab5 (Anand et al., 2003; “The Molecular Biology of Coronaviruses,”
17 2006) and that results in 16 NSPs (including itself) (Y. Chen et al., 2020) (**Scheme 1**). The
18 present study focused on the main protease in CoVs (3CL^{pro}/M^{pro}) (PDB ID 6LU7), as
19 potential target proteins for COVID-19 treatment. M^{pro} in COVID-19 has been structured and
20 repositioned in PDB and has been accessible by the public since early February 2020.
21 Mpro/3CLpro is active in its dimer state but till now there is no crystal structure available for
22 the dimer form. Its monomer inhabits the 306 amino acids including 3 domains, folded into
23 helices and β -strands. The electron density map for the monomer protein is clearly visible
24 (**Figure 1A**). The domain I (residues 1–101) and II (residues 102–184) includes an
25 antiparallel β -barrel structure; and domain III (residues 201–303) includes five α -helices
26 arranged into a largely antiparallel globular cluster, and is connected to domain II by means
27 of a long loop region (residues 185–200). The catalytic dyad (H41 and C145) is responsible
28 for the catalytic activity of SARS-COV-2 and is placed at the junction of domain I and
29 domain II (**Figure 1A**). Recently, a crystal structure for monomeric Mpro complexed with
30 N3 peptide like molecule (inhibitor) was crystallised (PDB-ID: 6LU7) and without any
31 inhibitor (PDB-ID: 6M03). The M^{pro} of 2019-nCov shares 96% similarity with the M^{pro} of the
32 SARS-CoV(Xu et al., n.d.; Zhavoronkov et al., n.d.). It is reported that 12 residues vary in
33 both SARS-CoV-1 and SARS-CoV-2 but the residue S46 in SARS-CoV-2 (COVID-19)
34 (corresponding residue A46 in SARS-CoV-1) is part of the binding site of the N3 molecule or
35 active site (Bzówka et al., n.d.) . A fragment molecular orbital (FMO) based interaction
36 analysis on a complex between the SARS-CoV-2 main protease (Mpro) and its peptide-like
37 inhibitor N3 (PDB ID: 6LU7) is reported. The target inhibitor molecule was segmented into
38 five fragments in order to capture site-specific interactions with amino acid residues of the
39 protease. From this study, H41, H163, H164, and E166 were found to be the key interacting
40 residue with the inhibitor, mainly due to hydrogen bonding (Hatada et al., n.d.). Another co-
41 crystal (PDB-ID 6Y2F), α -ketoamide inhibitor (13b) is also reported recently, providing the
42 structural and residue-based architecture of catalytic sites (L. Zhang et al., 2020). These co-
43 crystals are paving the route for the application of virtual screening to get more efficacious
44 molecules.

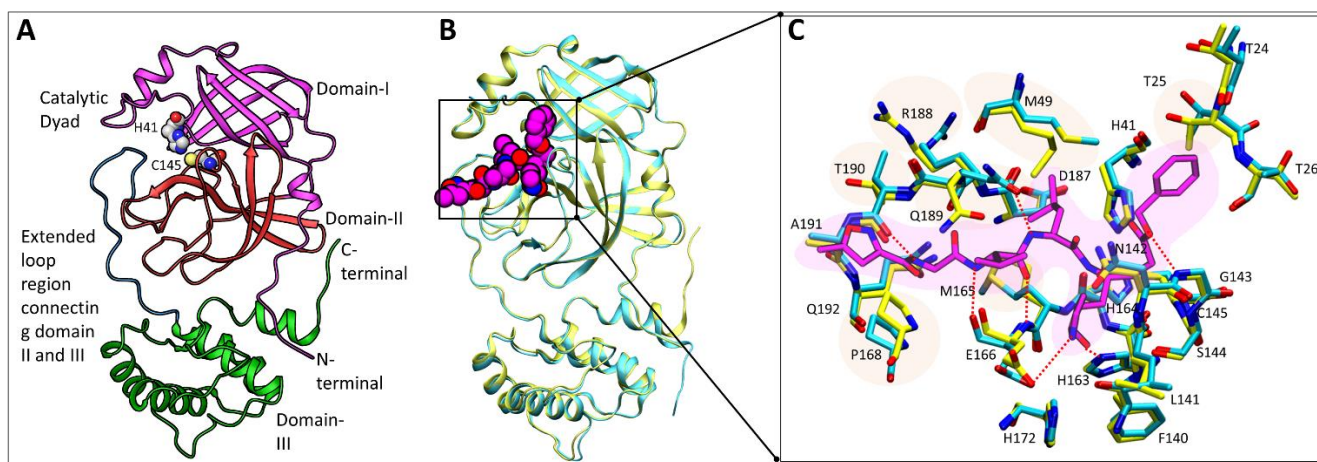
45



1

2 **Scheme1:** The schematic representation of non-structural proteins of SARS-CoV-2. The targeted protein M^{Pro}
 3 (main protease) is shown in red block. The modelled dimer was created. The crystal monomer 6LU7 was used
 4 for virtual screening and other post-processing analysis. **Rep** and **Prot** are repurpose and protease libraries.

5



6

7 **Figure 1:** Assessment of APO and COM structures of SARS-COV-2. (A) Overview of the APO structure
 8 (PDB-ID: 6M03), (B) Superimposition of APO (Yellow) and COM (Cyan) structure with peptide-like inhibitor
 9 represented in VdW and coloured in Purple, (C) Binding site alignment highlights the conformational difference
 10 in the residues. The residues are shown in licorice representation along with inhibitors shown in purple.

11

1 Considering the emergency situation, the drug repurposing approach is being widely applied
2 to quickly identify therapeutic solutions due to availability of their pharmacokinetic,
3 toxicological and manufacturing data. Drug repurposing includes drugs that are either FDA
4 approved, investigational, withdrawn or shelved molecules. Although there are studies of the
5 repurposing and marketed drugs which proposed several candidates for SARS-CoV-2
6 treatment (Contini, n.d.). With this aim, we have used a computer-aided drug design approach
7 to identify the new molecules against COVID-19. To facilitate the rapid identification of
8 potent molecules against COVID-19, we have performed the virtual screening of currently
9 FDA approved drugs, repurpose and anti-protease inhibitors of different viruses. The
10 findings from this study may provide opportunities to other researchers to identify and
11 develop the right molecules to combat against COVID-19.

12

13 **2. Materials and Methods**

14 **2.1 Protein Structure Preparation.** The protein crystals of M^{Pro} of Covid-19 were retrieved
15 from Protein Data Bank (PDB ID: 6LU7, 6M03) (Jin et al., n.d.). The crystal (6LU7) is found
16 to be bound with a peptide-like inhibitor 'N3' and another crystal (6M03) is without any
17 ligand (APO). The structures were optimized and then minimized using the Protein
18 Preparation Wizard module of Maestro (Anang et al., 2018; *Maestro, version 2017*;
19 *Schrödinger, LLC: New York, 2017*, n.d.) in which OPLS3 force field was used (Jorgensen et
20 al., 1996).

21 **2.2 SiteMap Analysis.** The SiteMap (*SiteMap, Version 4.2, Schrödinger, LLC, New York,*
22 *NY, 2017*, n.d.) program of Schrodinger Suite was also used for calculating binding sites on
23 crystal 6LU7. The method was implemented as an unbiased approach to undermine the
24 presence of any secondary or allosteric binding site. SiteMap which is a ligand independent
25 method, will also help in calculating the druggability of the identified site (Mattapally et al.,
26 2018; Srivastava et al., 2018). The method identifies putative binding sites by implementing
27 different parameters such as: *site score, size, exposure score, enclosure,*
28 *hydrophobic/hydrophilic character, contact, and donor/acceptor character* are considered to
29 highlight the potential binding site. As per Halgren analysis (Halgren, 2009), the average
30 number of sites for sub-micromolar sites is 132, where lower exposure scores of 0.52 and
31 Higher exposure scores of 0.76 average is considered better for sub-micromolar sites. For the
32 donor/ acceptor character and site score, the average for the sub-micromolar sites is 0.76 and
33 1.01, respectively. Druggability of the site is denoted by Dscore. Dscore values provide a
34 rough estimate of whether the site is druggable. These scores were derived by Halgren
35 (Halgren, 2009) by executing the SiteMap program on a number of proteins that have
36 inhibitors bound with potencies in the sub-micromolar range and performing statistical
37 analyses to produce optimized scores (Halgren, 2009). The OPLS-2005 force field (Jorgensen
38 et al., 1996) was employed, and a standard grid was used with 15 site points per reported site
39 and cropped at 4.0 Å from the nearest site point.

40 **2.3 Ligand Selection and Preparation.** The ligand structures were taken from
41 SELLEKCHEM database (<http://www.selleckchem.com/>), the DrugBank database
42 (<https://www.drugbank.ca/>) and the Repurposing hub (<https://clue.io/repurposing>) (see
43 Scheme 1). The ligands were prepared using Schrödinger's (version 2017-1), LIGPREP
44 (*LigPrep, version 4.2; Schrödinger, LLC: New York, 2017*, n.d.), which generates tautomers,
45 and possible ionization states at the pH range 7 ± 2 using Epik (*Epik Version 4.0,*
46 *Schrödinger, LLC, New York, NY, 2017*, n.d.) and also generates all the stereoisomers of the

1 ligand if necessary. The optimization was done using the OPLS3 force field (Jorgensen et al.,
2 1996). The pharmacokinetic descriptors of the hits were curated from the above-mentioned
3 databases.

4 **2.4 Virtual Screening of virtual libraries on M^{pro}.** The crystal used in this study was bound
5 with a peptide-like inhibitor which provided the primary site for ligand docking and also
6 SiteMap confirmed the primary site as the most druggable site. The grid was generated using
7 the centroid of bound inhibitor by using the Receptor Grid Generation panel in Glide.
8 Docking studies were carried out using the Virtual Screening Workflow (VSW) of Glide
9 Schrodinger Suite (Friesner et al., 2006; Mittal et al., 2020). The ligands chosen from the
10 database were passed through three stages of the screening workflow starting from high-
11 throughput screening (50% filtered), followed by standard precision (30%) and finally extra
12 precision (10%) stages. The final poses were processed using the Prime MM/GBSA panel at
13 the end (Schrodinger suite, LLC, New York, NY, 2016-3) (Scheme 1). The results of the
14 docking were then quantified on the basis of docking scores and MM/GBSA ΔG_{bind} .

15 **2.5 Figures.** All the images were generated using VMD and Schrodinger Suite (Asthana et
16 al., 2014, 2015; Humphrey et al., 1996).

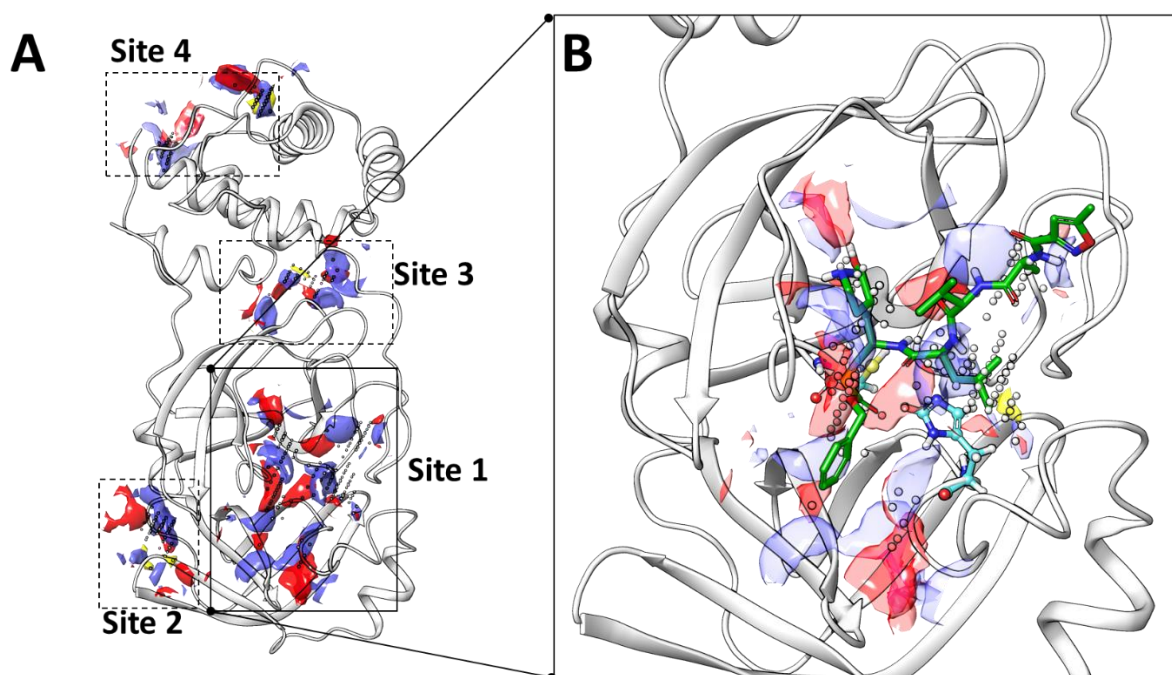
17

18 **3. Results and discussions**

19 **3.1 Comparative structural analysis:** The availability of co-crystal 6LU7 in which a
20 peptide (N3: a covalently-bonded inhibitor) is bound and knowledge of interacting residues
21 with molecule 13b (α -ketoamide inhibitor) made the understanding of protein interesting.
22 Since the M^{pro} is known to function in dimer state and compound 13b is reported to be bound
23 in dimer state, the crystal structure (coordinates file for PDB-ID: 6Y2F) for the same is not
24 available in RCSB Protein Data Bank so far. The residues reported for compound 13b
25 involve the same residues as for N3 molecule except for residue S1 from chain B. Therefore,
26 only monomer crystal was used for further analysis. The architecture of binding site with any
27 possible conformational changes was concurred after superimposition of the crystal structures
28 COM (6LU7) and APO (6M03). It shows that overall structure of protein is well aligned
29 (RMSD APO-vs.-COM is 0.4 Å) except C-terminal region (**Figure 1B**). We also observed
30 some noticeable differences in the binding site architecture of COM and APO (**Figure 1C**). It
31 was found that all the residues of the binding site are well aligned with that of APO except
32 the residues T25, M49, R188, T190, M165 and Q189 that shows side chain conformational
33 changes, while P168 shows the backbone movement also (Figure 1C). The inhibitor forms
34 the hydrogen bond (HB) interactions with residues G143, H163, E166, Q189, and T190.

35 **3.2 Exploring the druggable binding sites, docking and benchmark setup for compound**
36 **screening:** To bring in more robustness in confirming the final binding site before
37 performing the Virtual Screening, we performed ligand independent binding site search on
38 M^{pro}. The top score of the SiteMap program also confirms the co-crystal site as the primary
39 binding site (marked as Site 1) with the highest Dscore of 1.096 (best druggability score)
40 (**Figure 2 and Table 1**). The volume of the pocket is 287.09 Å³. This binding site of M^{pro} is
41 encompassed by domain I and II and the loop region connecting domains II and II. Sitemap
42 result shows that this pocket is relatively smaller in size with a size score of 120 (reference
43 value: 130), and more exposed to solvent with an exposure value of 0.614 (reference value:
44 0.52) (Halgren, 2009). Furthermore, we performed the focused docking on the Site 1 with the
45 N3 and 13b molecules to set up the benchmark for VS (Virtual screening) execution based on

1 two main criteria i.e docking score and MM-GBSA values. The docking score and MM-
2 GBSA values for N3 is -10.6 kcal/mol and -64.32 kcal/mol, respectively, while for 13b it is -
3 8.34 kcal/mol and -70.9 kcal/mol, respectively.



4

5 **Figure 2.** Possible binding sites and poses found by SiteMap. The yellow, red, and blue regions indicating the
6 hydrophobic, ligand acceptor and ligand donor sites, respectively

1 **Table 1:** SiteMap analysis on M^{PTO} monomer.

Title	SiteScore	size	D_score	Volume (Å³)	exposure	enclosure	contact	phobic	philic	balance	don/acc
site_1	1.02	120	1.09	287.09	0.61	0.65	0.87	1.21	0.71	1.70	0.86
site_2	0.64	41	0.59	116.62	0.76	0.55	0.78	0.27	1.03	0.27	0.60
site_3	0.65	30	0.45	106.33	0.63	0.68	1.00	0.17	1.44	0.12	0.56
site_4	0.61	25	0.56	73.75	0.75	0.59	0.72	0.73	0.79	0.91	4.17

2

3

4

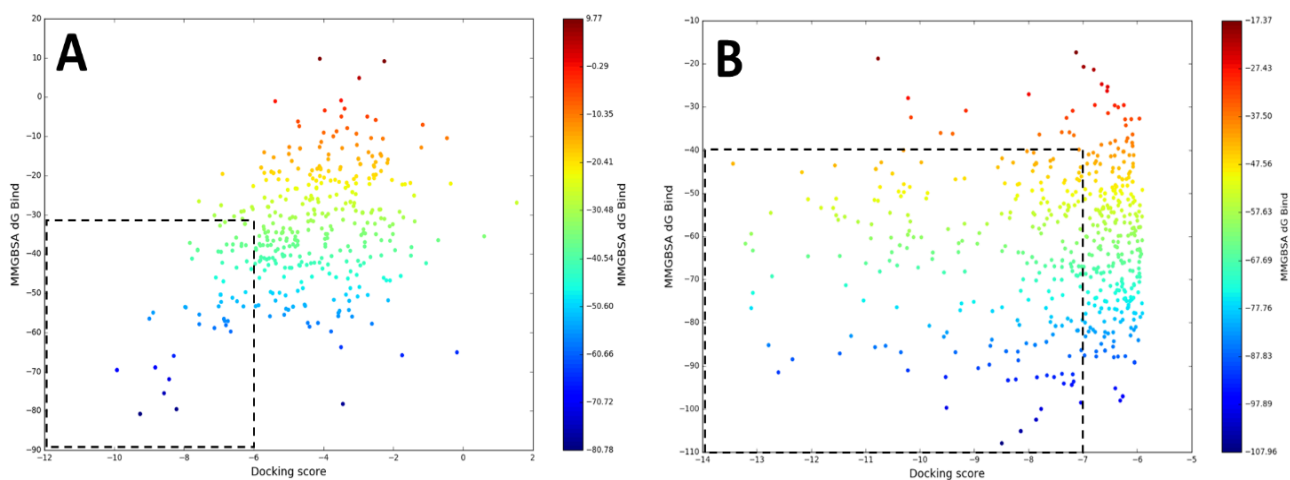
5

1

2 3.3 Virtual screening of two different libraries

3 **3.3.1 Protease library on the Site1 of M^{pro} protein:** It has been a proven and successful
4 strategy to inhibit the viral proteases for the treatment of viral infections such as in the cases
5 of human immunodeficiency virus (HIV) and hepatitis C virus (HCV) and hence screening of
6 protease inhibitors could be a useful approach against COVID-19 M^{pro} (Fischer et al., n.d.;
7 Ghosh et al., 2016; Yang et al., 2006). With this logic, 227 protease molecules from
8 Selleckchem were curated and prepared for screening on Site1. Based on our filtering criteria
9 of optimum MM/GBSA and docking scores, the top 30 initial hits were filtered out (**Figure**
10 **3A**). The docking scores, MM/GBSA, pharmacokinetic descriptors, their known targets,
11 along with the structures of the hits are shown in **Table 2**.

12 However, some of these molecules violate the pharmacokinetic properties but they can be
13 used as a starting point for the experimental validation and hits optimization that can facilitate
14 the identification of more potent drug-like molecules. For all selected molecules (top hits),
15 the residue mapping based on interaction pattern was executed (**Figure 4**). The top three
16 molecules found in our study are Leupeptin hemisulfate, pepstatin A and nelfinavir on the
17 basis of MM/GBSA and docking scores and their ligand interaction diagrams are shown in
18 **Figure 5A-5C** respectively. However, few of the molecules are observed to be common in
19 our screening and some in-silico studies published targeting M^{pro} and they are Nelfinavir,
20 Lopinavir, indinavir, ritonavir, darunavir (Adem et al., n.d.; Contini, n.d.; Farag et al., n.d.).



21

22 **Figure 3:** Scatter plot to calculate the docking scores (x-axis) and predicted MM-GBSA binding free energies
23 (kcal/mol) (y-axis) for hits obtained from virtual screening of (A) protease library (B) FDA/repurposed
24 molecules library. The points are coloured by MM-GBSA ΔG values. In plot (A) the total conformers obtained
25 after docking from 227 molecules protease library: 399 and in plot (B) total conformers reported after virtual
26 screening from 13947 FDA/repurposed library: 531

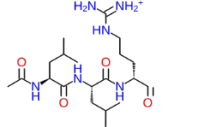
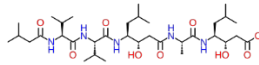
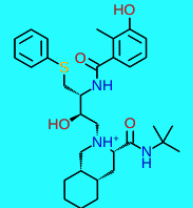
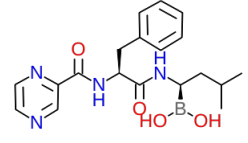
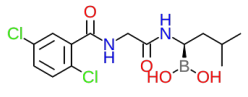
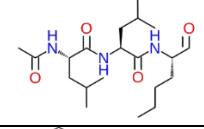
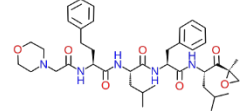
27

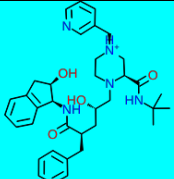
28

29

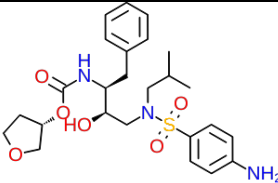
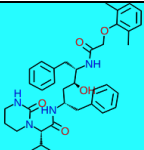
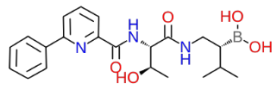
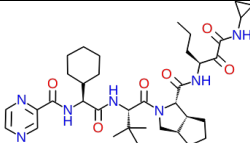
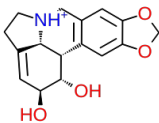

30

1 **Table 2:** Hits selected from proteases library along with their pharmacokinetic parameters and structures.

Name	Docking score	MMGBSA ΔG Bind	^a Mol Weight (g/mol)	Target	Developmental Phase	^b HBA	^c HBD	Rotatable bonds	^d PSA (\AA^2)	^e logP	^f logS	Structure
Leupeptin Hemisulfate	-9.257	-80.784	426.554	Serine Protease	Experimental	5	6	18	166.27	0.58	-3.72	
Pepstatin A	-9.919	-69.603	685.892	HIV Protease	Experimental	9	8	22	223	2.46	-4.19	
Nelfinavir	-8.822	-68.943	567.8	HIV Protease	Approved	5	4	10	101.9	4.61	-5.5	
Bortezomib (Velcade)	-8.291	-65.989	384.237	Proteasome	Approved	6	4	9	124.44	0.89	-3.9	
Ixazomib (MLN2238)	-6.658	-59.781	361.029	Proteasome	Approved, Investigational	4	4	7	98.66	2.57	-4.5	
MG-101 (ALLN) (calpain)	-7.126	-58.882	383.525	Cysteine Protease	Investigational	4	3	13	104	2.62	-3.07	
Carfilzomib (PR-171)	-6.795	-58.155	719.91	Proteasome	Approved, Investigational	8	4	20	158.47	4.2	-5.2	

L-685,458	-7.56	-57.905	672.853	Gamma-secretase	Experimental	6	5	22	159.8 5	4.76	-6.57	
Calpeptin	-6.74	-57.113	362.463	Cysteine Protease	Investigationa 1	4	2	12	84.5	3.23	-3.77	
Z-FA-FMK	-6.829	-57.077	386.417	Cysteine Protease	Experimental	5	2	12	84.5	2.46	-3.3	
Atazanavir	-6.853	-56.572	704.855	HIV Protease	Approved, Investigationa 1	7	5	18	171.2 2	4.54	-5.3	
ITF2357 (Givinostat)	-8.991	-56.502	475.965	HDAC	Investigationa 1	5	3	9	90.9	3.51	-4.9	
Indinavir	-7.946	-53.636	613.8	HIV Protease	Approved	7	4	12	118.0 3	2.81	-4.1	
LAQ824 (Dacinostat)	-7.965	-53.51	379.452	HDAC	Phase I	4	4	10	88.59	2.52	-3.42	
Anagliptin	-6.295	-53.377	383.447	DPP-4	Investigationa 1	6	2	6	115.4 2	-0.54	-3.3	
Aloin (Barbaloin)	-6.933	-52.231	418.394	Tyrosinase	Withdrawn	9	7	3	167.9 1	-0.14	-2.46	

LY411575	-6.477	-52.07	479.475	Gamma-secretase	Experimental	6	3	5	98.7	2.99	-4.63	
RG2833 (RGFP109)	-6.61	-51.173	339.431	HDAC	Experimental	3	3	8	84.2	3.04	-3.38	
Ritonavir	-6.949	-50.393	720.944	HIV Protease	Approved	6	4	18	145.78	5.22	-5.8	
E-64	-7.085	-46.011	357.405	Cysteine Protease	Experimental	6	5	11	172	-0.43	-0.8	
GI254023X	-6.492	-43.484	391.504	Immunology & Inflammation Related	NF*	4	3	10	98.7	2.65	-3.41	
Isorhamnetin	-6.901	-42.236	316.262	tyrosinase inhibitor	Experimental	7	4	2	116	1.65	-3.36	
TAPI-1	-7.768	-41.196	499.602	TNF-alpha protease inhibitor I	Experimental	6	6	13	163	1.75	-2.87	
Trelagliptin	-6.936	-39.477	357.382	DPP-4	Investigational	5	1	3	93.67	1.3	-3.2	

Amprenavir (Agenerase)	-6.61	-39.138	505.627	HIV Protease	Approved	6	3	11	131.1 9	2.43	-4	
Lopinavir (ABT-378)	-7.607	-38.997	628.801	HIV Protease	Approved	5	4	15	120	4.69	-5.5	
Delanzomib (CEP-18770)	-6.352	-37.975	413.275	Proteasome	Investigationa 1	6	5	9	131.7 8	2.57	-3.8	
Telaprevir	-6.78	-37.58	679.85	HCV proteases	Approved, Withdrawn	8	4	14	179.5 6	2.58	-4.3	
Lycorine	-6.502	-35.836	287.31	HCV proteases	Experimental	5	3	0	62.2	0.8	-2.54	
Darunavir	-6.9	-32.78	547.66	HIV Protease	Approved	7	3	11	140.4 2	2.82	-3.9	

1 The general recommended ranges are as follows:

2 ^aMolecular weight, <500.

3 ^bNumber of hydrogen bond acceptors, <10.

4 ^cNumber of hydrogen bond donors, <5.

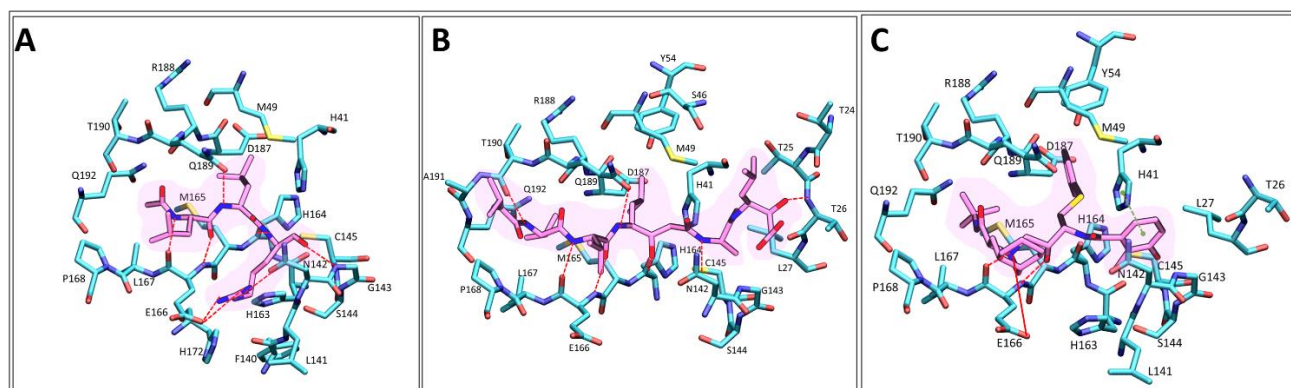
5 ^dPolar surface area, <140 Å²,

6 ^dPredicted octanol/water partition coefficient, -0.4 to +5.6.

7 ^ePredicted aqueous solubility, <-5.0.

8 *NF, not found

1



2

3 **Figure 5:** (A-C) the docked poses of Leupeptin Hemisulfate, Pepstatin A, Nelfinavir respectively within the
 4 binding site. Residues lining the pocket (Cyan) under 4.0 Å and its respective inhibitors (purple) are shown in
 5 licorice representation. Red and green dotted line shows the hydrogen bond and pi-pi interactions and red solid
 6 line means salt bridge.

7

8 **3.3.2 FDA/repurposing library on the Site1 of M^{pro} protein:** Another library of
 9 FDA/repurposing molecule curated from different sources such as repurposing hub,
 10 Selleckchem and DrugBank were used to prepare for screening purpose. FDA approved
 11 molecules are the fastest route to identify the active molecules. From the multi-step route of
 12 VS, we filtered out the best 41 hits (**Figure 3B**). The docking scores, MM/GBSA,
 13 pharmacokinetic descriptors, their known targets, along with the structures of the hits are
 14 shown in **Table 3** and their residue wise interaction mapping is also carried out (**Figure 6**).
 15 From this library, the best three molecules are Birinapant, Lypressin and Octreotide and their
 16 ligand interaction diagrams are shown in Figure 7A-7C respectively. Nevertheless, these
 17 molecules violate the pharmacokinetic properties but could be optimised to drug-like
 18 properties based on the experimental results. The finding of some common top molecules in
 19 this study are also reported in other screening studies on the same target, claiming the
 20 robustness of our protocols. These common molecules are Lypressin Octreotide,
 21 Mitoxantrone, Hesperidin, Echanoside, Pralmorelin, Epicatechin, Diosmin, Flavitan (flavin
 22 adenine dinucleotide), Curcumin, Saquinavir, Montelukast, Baicalin, Thymopentin (Adem et
 23 al., n.d.; Contini, n.d.; Farag et al., n.d.).

24

25

26

27

28

29

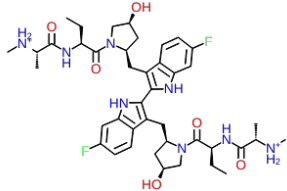
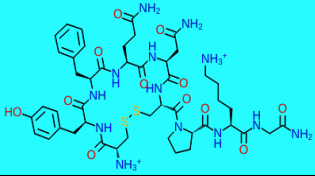
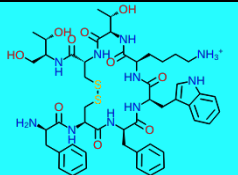
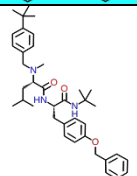
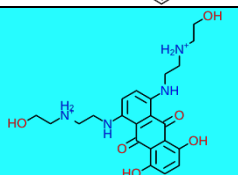
30

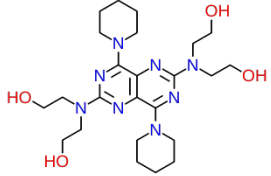
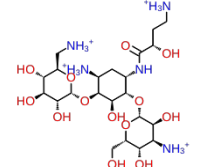
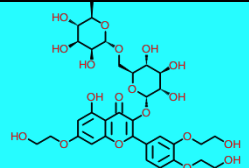
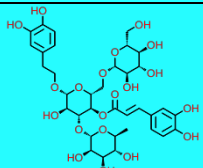
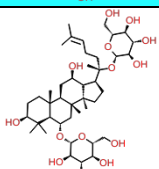
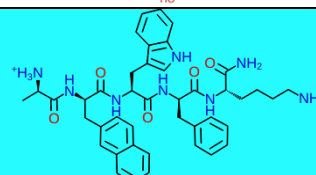
31

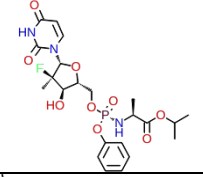
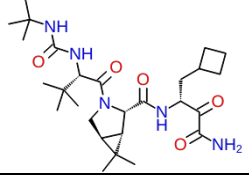
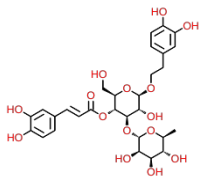
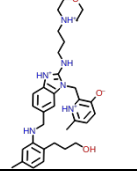
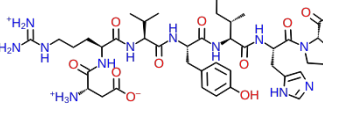
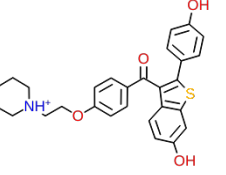
32

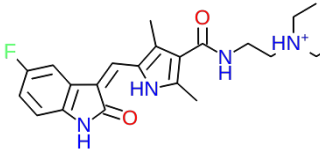
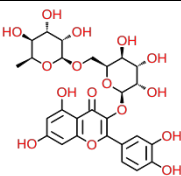
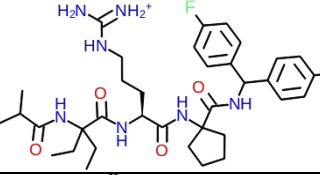
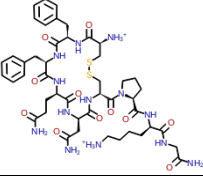

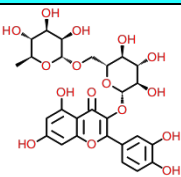
1

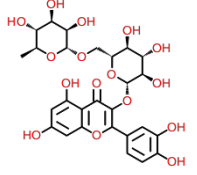

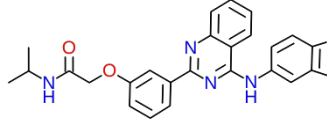
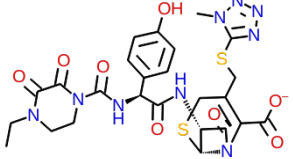
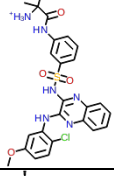
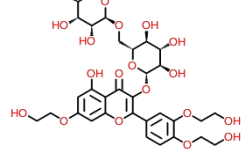
2 **Table 3:** Hits selected from FDA/Repurposed library along with their pharmacokinetic parameters and structures.

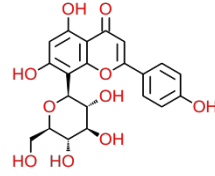
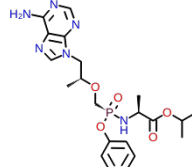
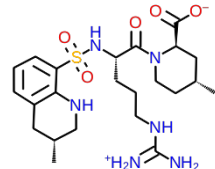
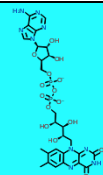
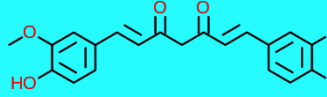

Title	Docking score	MMGBSA ΔG Bind	Phase	Source	^a MW	^b RB	^c PSA (\AA^2)	^d HB D	^e HBA	^f logP	^g logS	Pharmacological activity	Structures
Birinapant	-8.141	-105.15	Approved	drugbank	806.9	15	194.2	8	10	2.1	-4.6	peptidomimetic activator of SMAC and inhibitor of IAP; potential antineoplastic activity.	
Lypressin	-7.859	-102.499	Approved	drugbank	1056.2	19	452.9	16	24	2.2	-4.3	Antidiuretic hormone	
Octreotide	-7.202	-94.415	Approved	drugbank	1019.2	17	332.3	13	12	0.4	-4.9	potent inhibitor of growth hormone, glucagon, and insulin	
PD-173212	-7.168	-93.65	pre-clinical	repurhub	599.85	15	65.72	1	7	7.7	-9.08	calcium channel blocker	
Mitoxantrone	-8.232	-93.159	Approved	drugbank	444.5	12	163.1	8	10	0.9	-2.8	antineoplastic activity	

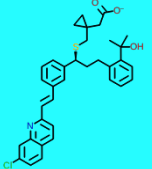
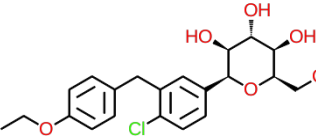
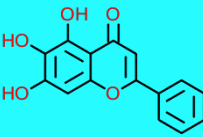
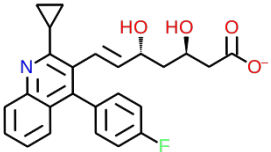
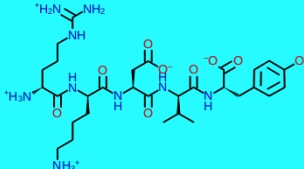
Dipyridamole (Persantine)	-7.184	-91.983	Approved	drugbank	504.6	12	145.4	4	12	1.5	-2.7	nucleoside transport inhibitor and a PDE3 inhibitor; inhibits blood clot formation	
Amikacin	-8.187	-88.745	Approved	drugbank	585.607	10	331.9	13	17	-8.6	-1.1	aminoglycoside antibacterial agent	
Hesperidin	-12.344	-88.5	Approved	drugbank	610.5	7	234.2	8	15	-0.2	-2.4	neurological conditions, antioxidant and anti-inflammatory effects	
Echinacoside	-11.473	-87.149	investigational	drugbank	786.7	14	324.4	12	19	-0.9	-2.3	Treatment of Neurological and other Disorders	
Ginsenoside Rg1	-10.349	-86.87	approved	repurposing hub	444.7	4	40.4	2	2	6.3	-6.4	antitumor, anti-inflammatory, antioxidation, and inhibition of cell apoptosis.	
Pralmorelin (GHRP-2)	-9.344	-86.865	phase II	repurposing hub	818	21	256	9	8	2.4	-5	Acts to endogenously increase growth hormone release from the pituitary.	

PSI-7976	-8.19	-86.73	pre-clinical	repurp hub	529.4 5	10	170.8 45	3	14	1.07	-3.71	HCV inhibitor	
Boceprevir	-7.028	-86.398	Approved, withdrawn	drugba nk	519.6	10	150.7	4	5	1.9	-4.4	HCV protease inhibitor (genotype 1).	
Acteoside	-10.631	-85.38	investigati onal	drugba nk	624.5	11	245.2	9	14	1	-2.8	a neuroprotective agent, an antileishmanial agent, an anti- inflammatory agent, a plant metabolite and an antibacterial agent.	
TMC353121	-11.266	-83.08	Approved	repurpo sing hub	558.7 27	13	107.7	4	6	4.09	-5.45	potent respiratory syncytial virus (RSV) fusion inhibitor	
TXA127	-9.5	-82.253	phase II	repurp hub	899.0 2	28	421.1 53	10	20	-2.93	-2.12	angiotensin receptor agonist	
Evista (Raloxifene Hydrochlori de)	-7.086	-81.815	approved, investigati onal	drugba nk	473.5	7	70	2	5	5.4	-6	Treatment of osteoporosis in postmenopausal women and those on glucocorticoids	

Sunitinib	-7.381	-80.705	approved	drugbank	398.4	7	77.2	3	3	3.2	-4.1	Used to treat certain types of advanced or progressive tumors of the stomach, intestines, esophagus, pancreas, or kidneys.	
Rutin	-13.104	-76.635	approved	drugbank	610.5	6	267	11	17	1.7	-3.1	radioprotective and antiplatelet activity. Rutin reduces hepatic and blood cholesterol levels.	
MM-102	-10.424	-76.45	pre-clinical	repurposing hub	669.8	21	178.3	7	7	2.85	-5.49	Peptidomimetic MLL1 inhibitor	
Felypressin	-8.486	-76.45	pre-clinical	drugbank	669.8	19	264.7	12	13	-1.1	-4.4	Non-catecholamine vasoconstrictor	
Epicatechin	-11.036	-74.878	investigational	drugbank	290.2	1	110.2	5	6	1	-2.6	Prevent the onset of type II diabetes and many cardiovascular diseases	
Quercetin 3-Rutinoside	-11.362	-71.34	Approved	drugbank	610.5	6	265.6	10	16	0.1	-2.2	antiallergic, anti-inflammatory, antiproliferative, and anticarcinogenic	

												properties	
Lanreotide	-8.097	-69.96	Approved	drugbank	1096.3	17	355	13	12	1.87	-5.3	management of acromegaly and symptoms caused by neuroendocrine tumors,	
Diosmin	-10.032	-67.23	Approved, investigational	drugbank	608.5	7	234.2	8	15	-0.4	-2.6	venous disease	
KD025 (Slx-2119)	-7.023	-66.999	phase II	repurposing hub	608.5	8	104.82	3	5	2.95	-5.7	Use idiopathic pulmonary fibrosis (IPF), selective ROCK2 inhibitor.	
Cefoperazone	-7.074	-66.95	Approved, investigational	drugbank	645.6	9	220.2	4	11	-0.1	-3.4	Effective against Pseudomonas infection and various bacterial infections.	
Pilaralisib	-7.691	-66.86	investigational	drugbank	541	7	148.3	4	8	3.98	-5	potential antineoplastic activity	
Troxerutin	-10.993	-66.24	investigational	drugbank	742.6	15	293.2	10	19	-0.5	-2.7	chronic venous insufficiency; vasoprotective	

Vitexin	-7.858	-65.995	investigational	drugbank	432.4	3	177	7	10	1.38	-2.8	platelet aggregation inhibitor, an antineoplastic agent and a plant metabolite.	
Tenofovir Alafenamide	-7.379	-65.61	Approved	drugbank	476.4	12	143.8	2	7	1.49	-3.3	treat chronic hepatitis B, and prevent HIV-1 infections	
Argatroban Monohydrate	-7.932	-64.8	Approved, investigational	drugbank	508.6	8	177.7	6	9	-0.9	-3.5	synthetic direct thrombin inhibitor derived from L-arginine	
Flavitan	-10.237	-62.71	Approved	drugbank	785.5	13	356	9	20	-2.7	-3.2	Vitamin B2 deficiency or metabolic disorder including stomatitis, eczema, etc	
Curcumin	-8.941	-61.71	Approved, Experimental, Investigational	drugbank	368.3	8	93	2	6	3	-4.3	chemopreventive and anticancer agents.	
Saquinavir	-7.461	-56.66	Approved, Investigational	drugbank	670.8	13	166.7	5	7	4	-5.4	anti-HIV protease inhibitor	

Montelukast	-7.418	-53.21	Approved	drugbank	586.1	12	70.4	2	4	7.2	-7.8	leukotriene antagonist, an anti-asthmatic drug and an anti-arrhythmia drug	
Dapagliflozin	-8.205	-50.56	Approved	drugbank	408.8	6	99.3	4	6	2.5	-3.4	sodium-glucose cotransporter 2 inhibitor	
Baicalein	-8.169	-47.81	pre-clinical	repurposing hub	270.2	1	87	3	5	1.7	-3.3	anti-inflammatory, antioxidant, antiviral, and antitumor effects, lipoxygenase inhibitor	
Pitavastatin	-8.435	-47.71	Approved	drugbank	421	8	90.6	3	5	3.75	-5	novel statin that induces plaque regression and elevates HDL-cholesterol levels	
Thymopentin	-8.026	-40.28	investigational	drugbank	679.9	22	327.6	11	14	-3.3	-4	treatment of rheumatoid arthritis, AIDS, and other primary immunodeficiencies.	

1 The general recommended ranges are as follows:

2 ^aMolecular weight, <500.

3 ^bRotatable bonds

4 ^cPolar surface area, <140 Å²,

5 ^dNumber of hydrogen bond donors, <5.

6 ^dNumber of hydrogen bond acceptors, <10.

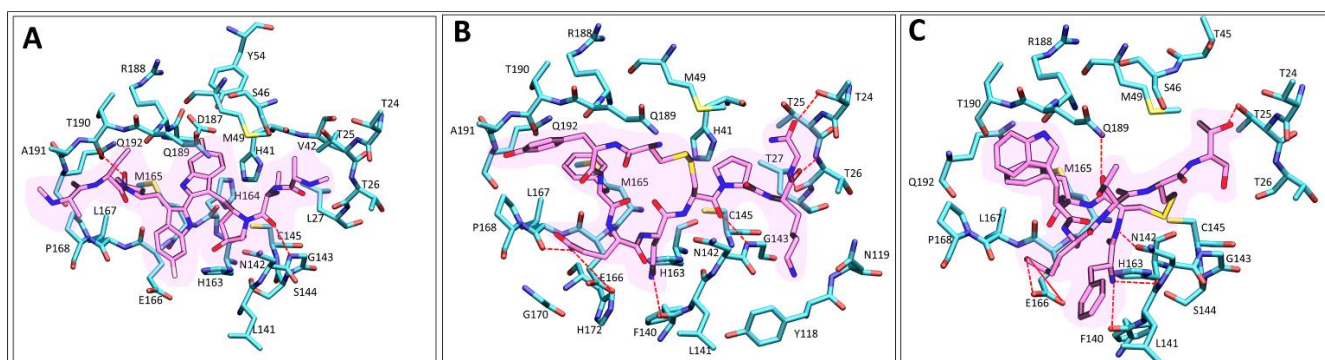
7 ^ePredicted octanol/water partition coefficient, -0.4 to +5.6.

8 ^fPredicted aqueous solubility, < -5.0.

9 *NF, not found

10 Blue highlighted cells are the molecules found common in screening results of other papers.

1



2

3 **Figure 7:** (A-C) The docked poses of Birinapant, Lypressin, Octreotide respectively within the binding site.
4 Residues lining the pocket (cyan) under 4.0 Å and its respective inhibitors (purple) are shown in licorice
5 representation. Red dotted line and red solid line shows the hydrogen bond and salt bridge interactions.

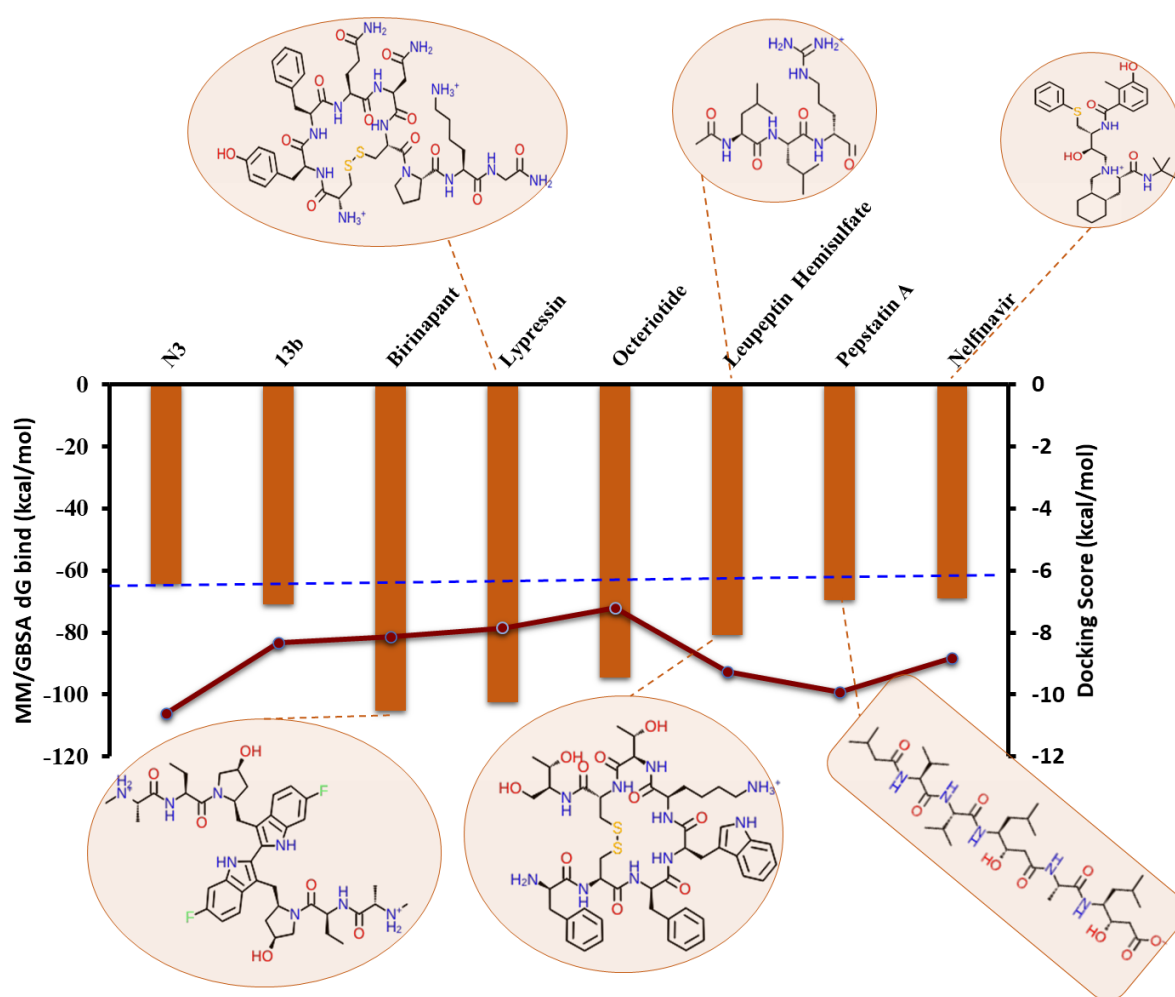
6

7 **3.4 Characterization of binding site:** The residues H41, M49, N142, C145, H164, M165,
8 E166, D187, R188 and Q189 having highest occupancy (>90%) for all the hits obtained from
9 protease library (**Figure 4**) with respect to the control compound N3. The residues G143,
10 E166, and Q189 are observed to be majorly involved in HBs (hydrogen bonds) interaction for
11 most of the hits while H41 is observed to form pi-pi stacking and pi-cation interaction in
12 some cases (**Figure 4**). Similarly, for the hits obtained from FDA/repurpose library, the
13 residue interaction mapping showed that the residues H41, M49, N142, C145, M165, E166,
14 R188, and Q189 have higher occupancy (>90%) in the binding site (**Figure 6**). The HBs
15 analysis found that residues T26, G143, E166, and Q189 are highly involved in the hydrogen
16 bond interaction (**Figure 6**). From the residue interaction mapping analysis of hits, we
17 observed that the static binding site of M^{Pro} is composed of 44.7% of polar residues, 42.1 %
18 of non-polar residues, 10.5% of acidic residues and 2.6% of basic residues which
19 encompasses a diverse class of molecules. This indicates that the binding site (site1) of M^{Pro}
20 is hydrophilic in nature and solvent exposed which is in concordance with our site map
21 results. However, the flexibility and adaptability of the pocket towards the ligand can be
22 further explored by molecular dynamics simulation studies. Interestingly, we find H41, M49,
23 N142, C145, H164, M165, E166 and Q189 are the most conserved residues and their
24 occupancy is 97-100% with all our top hits. As reported by Wang J. (Wang, n.d.) that MERS,
25 SARS and COVID-19 have four (H41, H163, M165 and Q189) common residues, while
26 HCV NS3/4A and COVID-19 have only one common hotspot residue (H41), confirming our
27 findings that the hits having interaction with these residues might have broad spectrum
28 value.

29 **3.5 Top rated molecules for in vitro analysis:** We identified six molecules with a lower free
30 energy of binding combined with a higher theoretical drug discovery value compared to the
31 co-crystallized ligand N3 and 13b (**Figure 8**). From the interaction pattern and other analysis,
32 the identified set of molecules should be considered as early hit molecules, albeit we accept
33 that no experimentally supported hit-optimization was conducted. Some molecules have
34 shown a minor decrease in their binding energies, also some of them have presented a
35 substantial improvement in comparison to the co-crystallized ligand. Different studies based
36 on virtual screening (Contini, n.d.), artificial intelligence (H. Zhang et al., n.d.) followed by
37 docking, neural network (Zhou et al., 2020) etc to discovery SARS-CoV-2 inhibitors we

1 observed that their docking scores ranging from -7.0 to -9.0 kcal/mol, however, Some of our
2 molecules have shown substantially good docking energy as well as their free energy is also
3 considerably higher side. Our identified antivirals interacted with the protease with at least
4 two HBs with an average of over four (**Figures 5 and 7**). From structure-based approaches
5 the knowledge of hot-spot residues is critical.

6 Furthermore, the identified molecules have shown relevant pharmacokinetic descriptors with
7 logP values, MW, PSA and hydrogen bond donors/acceptors in the range described by
8 Lipinski. Though we are aware that there are many FDA approved and successful candidates
9 who are documented that they are not following the standard Lipinski rule. It is interesting
10 that proposed inhibitors have shown their availability of molecules at commercial suppliers
11 such as MCULE and Selleckchem. The identified top six molecules presented comparatively
12 better docking and MM/GBSA scores with respect to the control molecules and therefore
13 represent excellent candidates for further investigation in vitro (**Figure 8**).



14

15 **Figure 8:** A plot of the MM/GBSA values (primary y-axis) and docking score (secondary y-axis) for the control
16 molecules and 6 finalized potential hits along with their 2D structures.

17

18 4. Conclusion

19 As the cases increase day by day there is an extremely urgent need of the designing small
20 compound or peptide drugs to cure the 2019-nCoV. A structure based virtual screening of

1 different known and existing molecule libraries was performed to identify useful molecules
2 that have potential to bind and could be repurposed against M^{Pro} of COVID-19. The protein-
3 ligand interaction analysis is suitable to overcome the challenge of screening thousands of
4 drugs in a short time in certain emergency situations, such as covid-19 outbreak. Considering
5 the current emergency situation for the need of effective drugs, our paper is more focused on
6 drug efficacy and their availability from different sources as they can be used immediately
7 skipping various time taking stages in the drug discovery and development pipeline. The
8 emergence of highly infectious SARS-CoV-2 is only possible to combat if we target this
9 deadly virus from different approaches as designed multiple treatment plans within a time
10 frame.

11 Computational drug repurposing study is known to provide treatment options in a short
12 period of time. Docking, ab-initio calculation, molecular modeling, needs CPU-GPU based
13 computational resources to compute and identify the potential possible molecule in target
14 dependent manner. We can run the drug repurposing screenings within four to five days using
15 a reliable HVS strategy. Depending upon the size of the M^{Pro} and the type of molecules it can
16 accommodate the screening time could be even optimised for it. The availability of high-
17 quality crystals of drug target structures is very important that can shed light into the
18 mechanistic insights of protein function. A high-resolution crystal structure of COVID-19
19 protease in complex with N3 and knowledge of key residues from 13b molecules (crystal is
20 not yet released) is available on time, allowing us to conduct this drug repurpose screening.
21 In absence of high-quality structure, one can rely on homology modeling technique, probably
22 with a reduced success rate of identifying repurposing drugs. We compared the crystal
23 structure of proteases of other SARS with COVID-19 and found that it is close to SARS-
24 COV-1.

25 In conclusion, we obtained some useful hit molecules from the structure-based virtual
26 screening having a binding energy of > -6.0 kcal/mol and MM/GBSA > -32.0 kcal/mol with
27 relevant ADME properties (**Table 2** and **Table 3**). Currently, antineoplastic,
28 immunomodulators, nucleotide inhibitors, antimalarial, ribonucleoside inhibitors, steroid
29 hormones, protease inhibitors, antiretrovirals are being evaluated in clinical trials against
30 COVID-19. Our screening molecules also belong to the similar category of molecules. The
31 hits found in our study belong to different chemical classes and have the potential to
32 accommodate inside the pocket that can be further validated by experimental assays. Our
33 interaction mapping has identified key interacting residues H41, M49, N142, C145, E166 and
34 Q189 and out of which H41 and C145 belong to the catalytic dyad. These hits or their
35 scaffolds can be used as a good starting point for developing novel hits by optimization or
36 can be used in combination treatments. The investigation of solvation sites or the role of
37 water molecules in the binding site could be carried out to explore the druggability of this
38 pocket that might help in rational designing of molecules. The potential candidate hits
39 provided in our paper can aid in facilitating the hunt of anti-covid-19 M^{Pro} drug discovery.
40 We believe that the structure-based virtual screening approach can play a vital role in
41 designing anti-coronaviral drugs.

42

43 **Acknowledgements**

44 The work has been supported by the facilities and support provided by THSTI.

45

1 **Author's Contribution**

2 S. Asthana proposed and designed the study. M. Srivastava, L. Mittal, A. Kumari and M.
3 Singh performed experiments and analysis of results. M. Srivastava, L. Mittal, A. Kumari and
4 S. Asthana wrote the manuscript.

5

6 **Conflicts of Interest**

7 The authors declare that they do not have conflict of interest.

8

References:

Adem, S., Eyupoglu, V., Sarfraz, I., Rasul, A., & Ali, M. (n.d.). *Identification of Potent COVID-19 Main Protease (Mpro) Inhibitors from Natural Polyphenols: An in Silico Strategy Unveils a Hope against CORONA*. <https://doi.org/10.20944/preprints202003.0333.v1>

Ahmed, M., Dwivedy, A., Mariadasse, R., Tiwari, S., Jeyakanthan, J., & Biswal, B. K. (n.d.). *Prediction of small molecule inhibitors targeting the novel coronavirus (SARS-CoV-2) RNA-dependent RNA polymerase*. <https://doi.org/10.31219/osf.io/fjnzc>

Anand, K., Ziebuhr, J., Wadhwani, P., Mesters, J. R., & Hilgenfeld, R. (2003). *Coronavirus Main Proteinase (3CLpro) Structure: Basis for Design of anti-SARS Drugs*. <https://doi.org/10.2210/pdb1p9t/pdb>

Anang, S., Kaushik, N., Hingane, S., Kumari, A., Gupta, J., Asthana, S., Shalimar, Nayak, B., Ranjith-Kumar, C. T., & Surjit, M. (2018). Potent Inhibition of Hepatitis E Virus Release by a Cyclic Peptide Inhibitor of the Interaction between Viral Open Reading Frame 3 Protein and Host Tumor Susceptibility Gene 101. *Journal of Virology*, 92(20). <https://doi.org/10.1128/JVI.00684-18>

Asthana, S., Shukla, S., Ruggerone, P., & Vargiu, A. V. (2014). Molecular mechanism of viral resistance to a potent non-nucleoside inhibitor unveiled by molecular simulations. *Biochemistry*, 53(44), 6941–6953. <https://doi.org/10.1021/bi500490z>

- Asthana, S., Zucca, P., Vargiu, A. V., Sanjust, E., Ruggerone, P., & Rescigno, A. (2015). Structure–Activity Relationship Study of Hydroxycoumarins and Mushroom Tyrosinase. In *Journal of Agricultural and Food Chemistry* (Vol. 63, Issue 32, pp. 7236–7244). <https://doi.org/10.1021/acs.jafc.5b02636>
- Bzówka, M., Mitusińska, K., Raczyńska, A., Samol, A., Tuszyński, J., & Góra, A. (n.d.). *Molecular Dynamics Simulations Indicate the SARS-CoV-2 Mpro Is Not a Viable Target for Small-Molecule Inhibitors Design*. <https://doi.org/10.1101/2020.02.27.968008>
- Cascella, M., Rajnik, M., Cuomo, A., Dulebohn, S. C., & Di Napoli, R. (2020). Features, Evaluation and Treatment Coronavirus (COVID-19). In *StatPearls*. StatPearls Publishing. <https://www.ncbi.nlm.nih.gov/pubmed/32150360>
- Chen, H., Guo, J., Wang, C., Luo, F., Yu, X., Zhang, W., Li, J., Zhao, D., Xu, D., Gong, Q., Liao, J., Yang, H., Hou, W., & Zhang, Y. (2020). Clinical characteristics and intrauterine vertical transmission potential of COVID-19 infection in nine pregnant women: a retrospective review of medical records. *The Lancet*, 395(10226), 809–815. [https://doi.org/10.1016/S0140-6736\(20\)30360-3](https://doi.org/10.1016/S0140-6736(20)30360-3)
- Chen, Y., Liu, Q., & Guo, D. (2020). Emerging coronaviruses: Genome structure, replication, and pathogenesis. *Journal of Medical Virology*, 92(4), 418–423. <https://doi.org/10.1002/jmv.25681>
- Chloroquine/ Hydroxychloroquine Prevention of Coronavirus Disease (COVID-19) in the Healthcare Setting - Full Text View - ClinicalTrials.gov*. (n.d.). Retrieved March 28, 2020, from <https://clinicaltrials.gov/ct2/show/NCT04303507>
- Contini, A. (n.d.). *Virtual Screening of an FDA Approved Drugs Database on Two COVID-19 Coronavirus Proteins*. <https://doi.org/10.26434/chemrxiv.11847381>
- Coronavirus*. (n.d.). Retrieved March 31, 2020, from https://www.who.int/health-topics/coronavirus#tab=tab_1

- Coronavirus Update (Live): 803,772 Cases and 39,070 Deaths from COVID-19 Virus Outbreak - Worldometer.* (n.d.). Retrieved March 31, 2020, from <https://www.worldometers.info/coronavirus/>
- Epik Version 4.0, Schrödinger, LLC, New York, NY, 2017.* (n.d.).
- Farag, A., Wang, P., Ahmed, M., & Sadek, H. (n.d.). *Identification of FDA Approved Drugs Targeting COVID-19 Virus by Structure-Based Drug Repositioning.* <https://doi.org/10.26434/chemrxiv.12003930.v1>
- Fischer, A., Sellner, M., Neranjan, S., Lill, M. A., & Smieško, M. (n.d.). *Inhibitors for Novel Coronavirus Protease Identified by Virtual Screening of 687 Million Compounds.* <https://doi.org/10.26434/chemrxiv.11923239.v1>
- Friesner, R. A., Murphy, R. B., Repasky, M. P., Frye, L. L., Greenwood, J. R., Halgren, T. A., Sanschagrin, P. C., & Mainz, D. T. (2006). Extra precision glide: docking and scoring incorporating a model of hydrophobic enclosure for protein-ligand complexes. *Journal of Medicinal Chemistry*, 49(21), 6177–6196. <https://doi.org/10.1021/jm051256o>
- Ghosh, A. K., Osswald, H. L., & Prato, G. (2016). Recent Progress in the Development of HIV-1 Protease Inhibitors for the Treatment of HIV/AIDS. *Journal of Medicinal Chemistry*, 59(11), 5172–5208. <https://doi.org/10.1021/acs.jmedchem.5b01697>
- Graham, R. L., Sparks, J. S., Eckerle, L. D., Sims, A. C., & Denison, M. R. (2008). SARS coronavirus replicase proteins in pathogenesis. In *Virus Research* (Vol. 133, Issue 1, pp. 88–100). <https://doi.org/10.1016/j.virusres.2007.02.017>
- Halgren, T. A. (2009). Identifying and characterizing binding sites and assessing druggability. *Journal of Chemical Information and Modeling*, 49(2), 377–389. <https://doi.org/10.1021/ci800324m>

- Hatada, R., Okuwaki, K., Mochizuki, Y., Fukuzawa, K., Komeiji, Y., Okiyama, Y., & Tanaka, S. (n.d.). *Fragment Molecular Orbital Based Interaction Analyses on COVID-19 Main Protease - Inhibitor N3 Complex (PDB ID:6LU7)*. <https://doi.org/10.26434/chemrxiv.11988120>
- Humphrey, W., Dalke, A., & Schulten, K. (1996). VMD: Visual molecular dynamics. *Journal of Molecular Graphics*, 14(1), 33–38. [https://doi.org/10.1016/0263-7855\(96\)00018-5](https://doi.org/10.1016/0263-7855(96)00018-5)
- Jin, Z., Du, X., Xu, Y., Deng, Y., Liu, M., Zhao, Y., Zhang, B., Li, X., Zhang, L., Peng, C., Duan, Y., Yu, J., Wang, L., Yang, K., Liu, F., Jiang, R., Yang, X., You, T., Liu, X., ... Yang, H. (n.d.). *Structure of Mpro from COVID-19 virus and discovery of its inhibitors*. <https://doi.org/10.1101/2020.02.26.964882>
- Jorgensen, W. L., Maxwell, D. S., & Tirado-Rives, J. (1996). Development and Testing of the OPLS All-Atom Force Field on Conformational Energetics and Properties of Organic Liquids. In *Journal of the American Chemical Society* (Vol. 118, Issue 45, pp. 11225–11236). <https://doi.org/10.1021/ja9621760>
- Kahn, J. S., & McIntosh, K. (2005). History and Recent Advances in Coronavirus Discovery. In *The Pediatric Infectious Disease Journal* (Vol. 24, Issue Supplement, pp. S223–S227). <https://doi.org/10.1097/01.inf.0000188166.17324.60>
- LigPrep, version 4.2; Schrödinger, LLC: New York, 2017.* (n.d.).
- Lu, H. (2020). Drug treatment options for the 2019-new coronavirus (2019-nCoV). *Bioscience Trends*. <https://doi.org/10.5582/bst.2020.01020>
- Maestro, version 2017; Schrödinger, LLC: New York, 2017.* (n.d.).
- Mattapally, S., Singh, M., Murthy, K. S., Asthana, S., & Banerjee, S. K. (2018). Computational modeling suggests impaired interactions between NKX2.5 and GATA4 in individuals carrying a novel pathogenic D16N NKX2.5 mutation. *Oncotarget*, 9(17), 13713–13732. <https://doi.org/10.18632/oncotarget.24459>

- Mittal, L., Kumari, A., Suri, C., Bhattacharya, S., & Asthana, S. (2020). Insights into structural dynamics of allosteric binding sites in HCV RNA-dependent RNA polymerase. *Journal of Biomolecular Structure & Dynamics*, 38(6), 1612–1625. <https://doi.org/10.1080/07391102.2019.1614480>
- Nair, D. t., & Narayanan, N. (n.d.). *Vitamin B12 may inhibit RNA-dependent-RNA polymerase activity of nsp12 from the COVID-19 Virus*. <https://doi.org/10.35543/osf.io/p48fa>
- SiteMap, Version 4.2, Schrödinger, LLC, New York, NY, 2017.* (n.d.).
- Srivastava, M., Suri, C., Singh, M., Mathur, R., & Asthana, S. (2018). Molecular dynamics simulation reveals the possible druggable of USP7. *Oncotarget*, 9(76), 34289–34305. <https://doi.org/10.18632/oncotarget.26136>
- Su, S., Wong, G., Shi, W., Liu, J., Lai, A. C. K., Zhou, J., Liu, W., Bi, Y., & Gao, G. F. (2016). Epidemiology, Genetic Recombination, and Pathogenesis of Coronaviruses. In *Trends in Microbiology* (Vol. 24, Issue 6, pp. 490–502). <https://doi.org/10.1016/j.tim.2016.03.003>
- The Molecular Biology of Coronaviruses. (2006). In *Advances in Virus Research* (Vol. 66, pp. 193–292). Academic Press. [https://doi.org/10.1016/S0065-3527\(06\)66005-3](https://doi.org/10.1016/S0065-3527(06)66005-3)
- Tirumalaraju, D. (2020a, March 17). *First US clinical trial of Covid-19 vaccine candidate begins*. Clinical Trials Arena. <https://www.clinicaltrialsarena.com/news/first-us-covid-19-vaccine-trial-moderna/>
- Tirumalaraju, D. (2020b, March 23). *China begins Phase I clinical trial of Covid-19 vaccine*. Clinical Trials Arena. <https://www.clinicaltrialsarena.com/news/china-covid-19-vaccine-trial-begins/>
- Tirumalaraju, D. (2020c, March 26). *Pfizer reports safety data of azithromycin in Covid-19 trial*. Clinical Trials Arena. <https://www.clinicaltrialsarena.com/news/pfizer-data-azithromycin-covid-19-trial/>

- Wang, J. (n.d.). *Fast Identification of Possible Drug Treatment of Coronavirus Disease -19 (COVID-19) Through Computational Drug Repurposing Study*.
<https://doi.org/10.26434/chemrxiv.11875446.v1>
- Xu, Z., Peng, C., Shi, Y., Zhu, Z., Mu, K., Wang, X., & Zhu, W. (n.d.). *Nelfinavir was predicted to be a potential inhibitor of 2019-nCov main protease by an integrative approach combining homology modelling, molecular docking and binding free energy calculation*.
<https://doi.org/10.1101/2020.01.27.921627>
- Yang, S., Chen, S.-J., Hsu, M.-F., Wu, J.-D., Tseng, C.-T. K., Liu, Y.-F., Chen, H.-C., Kuo, C.-W., Wu, C.-S., Chang, L.-W., Chen, W.-C., Liao, S.-Y., Chang, T.-Y., Hung, H.-H., Shr, H.-L., Liu, C.-Y., Huang, Y.-A., Chang, L.-Y., Hsu, J.-C., ... Hsu, M.-C. (2006). Synthesis, Crystal Structure, Structure–Activity Relationships, and Antiviral Activity of a Potent SARS Coronavirus 3CL Protease Inhibitor. In *Journal of Medicinal Chemistry* (Vol. 49, Issue 16, pp. 4971–4980). <https://doi.org/10.1021/jm0603926>
- Zhang, H., Saravanan, K. M., Yang, Y., Hossain, M. T., Li, J., Ren, X., & Wei, Y. (n.d.). *Deep Learning Based Drug Screening for Novel Coronavirus 2019-nCov*.
<https://doi.org/10.20944/preprints202002.0061.v1>
- Zhang, L., Lin, D., Sun, X., Curth, U., Drosten, C., Sauerhering, L., Becker, S., Rox, K., & Hilgenfeld, R. (2020). Crystal structure of SARS-CoV-2 main protease provides a basis for design of improved α -ketoamide inhibitors. *Science*. <https://doi.org/10.1126/science.abb3405>
- Zhavoronkov, A., Aladinskiy, V., Zhebrak, A., Zagribelnyy, B., Terentiev, V., Bezrukov, D. S., Polykovskiy, D., Shayakhmetov, R., Filimonov, A., Orekhov, P., Yan, Y., Popova, O., Vanhaelen, Q., Aliper, A., & Ivanenkov, Y. (n.d.). *Potential 2019-nCoV 3C-like Protease Inhibitors Designed Using Generative Deep Learning Approaches*.
<https://doi.org/10.26434/chemrxiv.11829102.v1>

Zhou, Y., Hou, Y., Shen, J., Huang, Y., Martin, W., & Cheng, F. (2020). Network-based drug repurposing for novel coronavirus 2019-nCoV/SARS-CoV-2. *Cell Discovery*, 6, 14. <https://doi.org/10.1038/s41421-020-0153-3>